

An information-based metric for observing strategy optimization, demonstrated in the context of photometric redshifts with applications in cosmology

Alex I. Malz,^{1*} Francois Lanusse,² John Franklin Crenshaw,³ & Melissa L. Graham⁴

¹*Ruhr-University Bochum, German Centre for Cosmological Lensing, Universitätsstraße 150, 44801 Bochum, Germany*

²*AIM, CEA, CNRS, Université Paris-Saclay, Université Paris Diderot, Sorbonne Paris Cité, F-91191 Gif-sur-Yvette, France*

³*Department of Physics, University of Washington, Box 351560, Seattle, WA 98195*

⁴*DiRAC Institute, Department of Astronomy, University of Washington, Box 351580, U.W., Seattle, WA 98195, USA*

Accepted XXX. Received YYY; in original form ZZZ

ABSTRACT

The observing strategy of a galaxy survey influences the degree to which its resulting data can be used to accomplish any science goal. LSST is thus seeking metrics of observing strategies for multiple science cases in order to optimally choose a cadence. Photometric redshifts are essential for many extragalactic science applications of LSST’s data, including but not limited to cosmology, but there are few metrics available, and they are not straightforwardly integrated with metrics of other cadence-dependent quantities that may influence any given use case. We propose a metric for observing strategy optimization based on the potentially recoverable mutual information about redshift from a photometric sample under the constraints of a realistic observing strategy. We demonstrate a tractable estimation of a variational lower bound of this mutual information implemented in a public code using conditional normalizing flows. By comparing the recoverable redshift information across observing strategies, we can distinguish between those that preclude robust redshift constraints and those whose data will preserve more redshift information, to be generically utilized in a downstream analysis. We recommend the use of this versatile metric to observing strategy optimization for redshift-dependent extragalactic use cases, including but not limited to cosmology, as well as any other science applications for which photometry may be modeled from true parameter values beyond redshift. †

Key words: surveys – galaxies: distances and redshifts – methods: statistical

1 INTRODUCTION

The Vera C. Rubin Observatory will produce a catalog of tens of billions of astronomical objects over the course of the ten-year Legacy Survey of Space and Time (LSST; Ivezić et al. 2019). The quality and quantity of resulting data will depend on LSST’s observing strategy (OS), which encompasses the choice of frequency and duration of visits to each portion of the night sky across each of LSST’s *ugrizy* filters as a function of the survey’s duration. As the OS directly impacts the science one can accomplish with the resulting data (Jones et al. 2020), LSST’s Science Collaborations (SCs) are directing considerable effort to optimizing the choice of OS (e.g., LSST Science Collaboration et al. 2017; Graham et al. 2018; Lochner et al. 2021, to name but a few).

Though the space of all OSs is very high-dimensional, a decision of OS may be informed by how each science goal is affected by each OS considered. LSST has developed two tools¹ to facilitate an optimal choice of OS. OpSim (LSST 2016; Delgado et al. 2014) forecasts the impact of an OS on the properties of the resulting photometric observations LSST will deliver. The MAF (Metrics Analysis Frame-

work) (LSST 2017) was established to ensure that the choice of OS would be well-informed by all science cases, whose proponents are invited to include one or more metrics to be automatically evaluated for each set of simulated observational conditions. Though each science application may favor a different OS, a fair choice may be made by reviewing how all science goals are affected.

The utility of a gargantuan catalog of extragalactic objects, such as what LSST will provide, relies on the accuracy and precision of its constraints on their redshifts, which, for a photometric survey such as LSST, represent a dominant factor in the error budgets of most if not all extragalactic science applications. Without access to high-fidelity spectroscopic redshift measurements, users of LSST’s extragalactic catalog will rely on photometric redshift (photo-*z*) estimates, which suffer from multiple forms of uncertainty, even under idealized conditions (see Schmidt et al. 2020, and extensive references therein).

Redshift uncertainty thus represents one of LSST’s greatest liabilities and one of the utmost importance to multiple LSST SCs (Awan et al. 2016; Lochner et al. 2018; Scolnic et al. 2018; Almoubayyed et al. 2020), particularly the Dark Energy SC (DESC), Transients and Variable Stars (TVS) SC, and Galaxies SC, but photo-*z* metrics remain underdeveloped. Some metrics are straightforward, such as the 10-year coadded depth or the number of supernovae with more than 10 epochs, and can be directly predicted from the OpSim

* E-mail: aimalz@astro.ruhr-uni-bochum.de

¹ <https://pstn-051.lsst.io/>

metadata and visualized as sky maps with HEALpix (Górski et al. 2005). However, photo- z performance is quantified by derived statistics of a particular photo- z estimator on an entire simulated galaxy catalog, often as a function of true redshift. The holy grail of OS metrics would be a map of “goodness of photo- z quality” insensitive to photo- z estimator for each HEALpix pixel, a goal that has not yet been achieved, let alone with enough computational efficiency for practical MAF integration.

Multiple aspects of the current approach to photo- z metrics for OS optimization would benefit from improvement, ideally addressing as many as possible of the following needs:

- An observing strategy metric for photo- z s should be agnostic to the choice of estimation method as well as whether point estimates or photo- z posteriors are used.
- A metric for photo- z should be adaptable to integrate with metrics of additional quantities sensitive to observing strategy.
- An observing strategy metric for photo- z s should not preclude direct comparison of overall metrics between science goals nor between analysis approaches for a shared science goal.
- Any metric included in the MAF should be fast and scalable; simulation and propagation of mock data through an entire analysis pipeline is not feasible.

This paper explores a potential OS metric of estimated redshift quality that represents an improvement upon established metrics along the above axes. Our metric relies directly on estimating the mutual information between photometry and redshift, in other words, quantifying how much information is gained on the redshift of galaxies by having access to the photometry under a given OS.

This paper is not the first use of an information criterion for optimization in the context of redshift estimation. Malz et al. (2018) used an information-theoretic metric to optimize the storage parameterization of photo- z posteriors, however, Kalmbach et al. (2020) used a metric of mutual information more closely related to that of this work to optimize filter design for photo- z s. In their work, photometric data with Gaussian error was simulated using a simple redshift prior and a small number of galaxy SED templates. This simple forward model provided an analytic method for calculating the mutual information.

In this paper, we leverage recent advances in machine learning to enable the calculation of the mutual information contained in more complex simulations for which an analytic model may be unavailable, as could be anticipated of even idealized data processed through OpSim under a realistically complex OS. In Section 2, we introduce the mathematical framework for the variational mutual information lower bound that serves as the basis for our metric. In Section 3, we demonstrate the metric in the context of OS optimization for LSST. And in Section 4, we summarize its strengths and future directions for its development and application.

2 METHOD: VARIATIONAL MUTUAL INFORMATION LOWER BOUND

This section introduces TheLastMetric (TLM), denoted as \mathfrak{T} ,² an estimator-independent metric for parameters of interest conditioned on photometry under any OS. Though we derive it in the context of redshift-dependent cosmological probes, its mathematical structure is not inherently restricted to redshift; as it is so broadly applicable across science cases, one may jokingly exaggerate that it’s the penultimate OS metric, hence its name.

² the last letter of the Hebrew alphabet, pronounced “tav”

In Section 2.1, we introduce the mathematical formalism and review relevant information-theoretic concepts. In Section 2.2 we derive the metric itself, and in Section 2.3 we describe the model by which the metric is calculated.

2.1 An information theoretic view of observing strategies

Every science case seeks a metric of how informative the data corresponding to each OS is with respect to some physical parameters of interest. The properties of the telescope and its OS correspond to a transformation of the underlying true data in the universe. Such true data would correspond to photons that could be observed only by an impossibly perfect, idealized instrument that collects complete, noiseless data, in contrast to what we can observe from any real telescope under a given OS, a subset of those photons restricted by the OS and convolved with instrumental errors. Typically, the information content of recovered physical parameters is determined by running the observed data through an end-to-end analysis pipeline, which is impractical for a MAF. This is particularly true for cosmological applications, but while our derived cosmological constraints depend on the analysis procedure (Chang et al. 2018), the potentially recoverable cosmological information content does not.³

Let us begin by quantifying the total cosmological information content of an idealized survey with perfect photometry using information theory. We denote the random variable representing cosmological parameters as Θ and a random variable representing survey photometry as X_{phot} . The information content about cosmological parameters $\theta \sim \Theta$ due to photometry $x_{phot} \sim X_{phot}$ can be described by the *mutual information* between Θ and X_{phot} , defined as

$$I(\Theta; X_{phot}) \equiv \mathbb{E}_{p(\theta, x_{phot})} \left[\log \frac{p(\theta, x_{phot})}{p(\theta)p(x_{phot})} \right]. \quad (1)$$

The mutual information between two random variables represents the reduction in uncertainty in one due to knowing the other. It is desirable for this mutual information to be large, i.e. we want the photometry x_{phot} to be very informative about the cosmological parameters θ .

In practice, of course, we do not have access to perfect photometry, and a typical cosmological analysis pipeline does not directly relate photometry to cosmology in a single step; instead, typical analyses constitute a pipeline from observed photometry X_{phot}^{obs} to cosmology Θ via a number of intermediate quantities. The relationship between cosmological parameters Θ , redshift distribution Z , true photometry X_{phot}^{true} , and observed photometry X_{phot}^{obs} is an example of a Markov chain $\Theta \rightarrow Z \rightarrow X_{phot}^{true} \rightarrow X_{phot}^{obs}$ satisfying

$$p(\theta, z, x_{phot}^{true}, x_{phot}^{obs}) = p(\theta) p(z|\theta) p(x_{phot}^{true}|z) p(x_{phot}^{obs}|x_{phot}^{true}). \quad (2)$$

The amount of information each stage of this chain retains about cosmology can be expressed using the *data processing inequality* (Cover & Thomas 2006),

$$I(\Theta; Z) \geq I(\Theta; X_{phot}^{true}) \geq I(\Theta; X_{phot}^{obs}), \quad (3)$$

³ Though we derive and demonstrate our metric with this application in mind, such a statement is no less true of other physical parameters of interest to a variety of science cases, making this metric broadly applicable beyond cosmology or even redshifts.

which can be intuitively understood as saying that information can only be lost through the steps of a chain.

Every application of LSST data aims to minimize the information loss in the steps of this chain, or one analogous to it, that are under our control. An example of a step we as experimenters control is the choice of OS that min information loss in the stages of this chain that relates galaxies' true redshifts and their observed photometry $I(Z; X_{phot}^{obs})$, which depends on the specific OS that transforms $X_{phot}^{true} \rightarrow X_{phot}^{obs}$. Again following the data processing inequality, we expect the following:

$$I(Z; X_{phot}^{true}) \geq I(Z; X_{phot}^{obs}), \quad (4)$$

i.e. that the mutual information between redshift and observed photometry would be saturated if perfect, true, unobservable photometry were available, but the OS determines how closely we can approximate that bound.

Our goal is to compare the mutual information $I(Z; X_{phot}^{obs})$ ⁴ for different OSs, with the understanding that the OS that can achieve the highest mutual information at this level of the chain will also maximize the overall mutual information with respect to cosmology $I(\Theta | X_{phot}^{obs})$ for a fixed analysis pipeline. Given this scope, we henceforth use X_{phot} as shorthand for X_{phot}^{obs} . The next challenge to discuss is a practical computation of the mutual information.

2.2 Tractable variational lower bound on the mutual information

Evaluating the mutual information as defined in Equation 1 is in general extremely challenging, as in most cases only samples from the distributions involved as accessible, not the underlying distributions themselves. In recent years however, the concept of mutual information has found many applications in the machine learning literature (e.g. Tishby & Zaslavsky 2015; Alemi et al. 2017; Bachman et al. 2019, as well as the recent review of Poole et al. (2019)), which has driven significant research into tractable estimators of lower bounds.

To achieve a tractable expression for the mutual information $I(Z; X_{phot})$ of redshift and photometry, let us first introduce the *entropy*

$$H(Z) \equiv - \int dz p(z) \log p(z) \quad (5)$$

of the redshift distribution $p(z)$, which quantifies our uncertainty on the random variable Z . Using Equation 5, we rewrite the mutual information $I(Z; X_{phot})$ of redshift and photometry in the following way:

$$\begin{aligned} I(Z; X_{phot}) &= \mathbb{E}_{p(z, x_{phot})} \left[\log \frac{p(z|x_{phot})}{p(z)} \right] \\ &= \mathbb{E}_{p(z, x_{phot})} [\log p(z|x_{phot})] - \mathbb{E}_{p(z)} [\log p(z)] \\ &= \mathbb{E}_{p(z, x_{phot})} [\log p(z|x_{phot})] + H(Z). \end{aligned} \quad (6)$$

As we do not directly have access to the posterior distribution $p(z|x_{phot})$, the first term is unknown, making the mutual information itself intractable.

However, the overall expression for the mutual information can

be bounded from below by introducing a variational approximation $q_\varphi(z|x_{phot})$ for the posterior $p(z|x_{phot})$, which leads to the variational lower bound introduced in Barber & Agakov (2003):

$$\begin{aligned} I(Z; X_{phot}) &= \mathbb{E}_{p(z, x_{phot})} \left[\log \frac{p(z|x_{phot})}{q_\varphi(z|x_{phot})} \right] \\ &+ \mathbb{E}_{p(z, x_{phot})} [\log q_\varphi(z|x_{phot})] + H(Z) \end{aligned} \quad (7)$$

$$\begin{aligned} &= \mathcal{D}_{KL} [p(z|x_{phot}) || q_\varphi(z|x_{phot})] \\ &+ \mathbb{E}_{p(z, x_{phot})} [\log q_\varphi(z|x_{phot})] + H(Z). \end{aligned} \quad (8)$$

In this expression, $\mathcal{D}_{KL} [p(z|x_{phot}) || q_\varphi(z|x_{phot})]$ is the Kullback-Leibler Divergence (KLD), a directional measure of the loss of information due to using the variational model $q_\varphi(z|x_{phot})$ as an approximation to the true, unknown, posterior distribution $p(z|x_{phot})$. Because this KLD is non-negative, this last expression can be used to provide the following lower bound on the mutual information:

$$I(Z; X_{phot}) \geq \mathbb{E}_{p(z, x_{phot})} [\log q_\varphi(z|x_{phot})] + H(Z) \equiv \mathfrak{N}, \quad (9)$$

thereby providing the definition of TheLastMetric (TLM).

Not only is this expression now tractable, as it can be estimated simply by *optimization* of the variational parameters φ , but, moreover, the bound is tight when $q_\varphi(z|x_{phot}) = p(z|x_{phot})$ is true. Like the KLD, \mathfrak{N} has units of information, which are *nats* in the base-*e* convention used in this paper but can be trivially converted to, e.g. base-2 *bits*.

2.3 Lower bound implementation using conditional normalizing flows

The lower bound on mutual information introduced in the previous section relies on having access to a parametric conditional density $q_\varphi(z|x_{phot})$, also known as the variational distribution, which is optimized to match the true posterior $p(z|x_{phot})$. Any parametric conditional density estimator could be used for this purpose, but the more expressive the model, the tighter the lower bound will be.

In this work, we approximate $p(z|x_{phot})$ with a Normalizing Flow (NF) (Jimenez Rezende & Mohamed 2015; Dinh et al. 2015), a flexible class of deep generative models that represents the current state-of-the-art on many density estimation tasks (Kobyzev et al. 2020). NFs are Latent Variable Models (LVMs), which model a given distribution $p(x)$ over a target variable x by introducing 1) a latent variable z that follows a known prior distribution (typically a multivariate normal distribution) $p(z)$ as $z \sim p(z)$ and 2) a parametric mapping f_φ that maps this latent variable z to a point in the target distribution x according to $x = f_\varphi(z)$. This is no different from other deep generative latent variable models like Variational Autoencoders (Kingma & Welling 2013) or Generative Adversarial Networks (Goodfellow et al. 2014), but what sets NFs apart is that they are specifically designed using a *bijective* mapping f_φ . In the case of a bijection, the probability density function q_φ of the model can be expressed as

$$q_\varphi(x) = p(z = f_\varphi^{-1}(x)) \left| \det \frac{\partial f_\varphi}{\partial x}(x) \right|^{-1}, \quad (10)$$

where $\det \frac{\partial f_\varphi}{\partial x}$ is the Jacobian determinant of f_φ , which accounts for how f_φ distorts volume elements. This expression is nothing more than the change of variable formula for probabilities, but it gives NFs a crucial advantage over other LVM models: their probability density function has an explicit closed-form expression. In other words, for a given set of parameters φ we can explicitly compute the probability $q_\varphi(x)$ of a data point x under the model.

A Conditional NF (CNF) can be trivially made by introducing a

⁴ As was suggested in the preamble, this paper concerns the mutual information of redshift and photometry, but the derivation is just as valid for the mutual information $I(\Psi; X_{phot}^{obs})$ of observed photometry with some other parameter Ψ , for example e.g. stellar mass, used in any science application, even beyond cosmology.

conditional variable y in the mapping $f_\varphi(z; y)$ (Winkler et al. 2019) that preserves the bijectivity of the mapping for all y , so Equation 10 still applies. Thus the conditional distribution modeled by the flow is simply:

$$q_\varphi(x|y) = p(z = f_\varphi^{-1}(x; y)) \left| \det \frac{\partial f_\varphi}{\partial x}(x; y) \right|^{-1}. \quad (11)$$

In practice, as the mapping f_φ is typically implemented using a neural network, making a normalizing flow conditional simply amounts to adding the variable y as an input to the networks parameterizing the flow.

Because (C)NFs have tractable likelihoods, they can be trained by directly optimizing the probability of the training set under the model. For CNFs, the training loss takes the following form

$$\mathcal{L} = -\mathbb{E}_{p(x, y)} [\log q_\varphi(x|y)], \quad (12)$$

which can be shown to minimize the KLD $\mathcal{D}_{KL}[p(x|y)||q_\varphi(x|y)]$, i.e. driving the (approximating) model distribution to be close to the (true) data distribution. We note that the CNF’s loss function given by Equation 12 is equal to the first term of the variational lower bound Equation 7. In other terms, training the CNF with this loss function is exactly equivalent to maximizing the variational mutual information lower bound.

The approach presented here to build a practical lower bound is agnostic to the NF architecture employed, but the specific choice should be appropriate to the details of the problem at hand. We defer the details of the model used in this work to Section 3.2.

3 DEMONSTRATION IN THE CONTEXT OF REDSHIFTS FOR LSST

The necessary and sufficient conditions favoring the use of TLM are that it must be at least as effective as established metrics and have some additional advantage(s), such as utility, interpretability, and/or efficiency. To demonstrate the former, we perform controlled experiments on appropriate data, described in Section 3.1, using an implementation of a variational approximation to \mathfrak{N} , presented in Section 3.2. The latter is discussed in Section 3.3, where the results of this experiment are presented.

3.1 Data: simulated photo- z catalogs

For this work, we use simulations based on the same mock galaxy catalog to which the Color-Matched Nearest-Neighbors (CMNN) photo- z estimator⁵ was applied to produce LSST-like photo- z results in Graham et al. (2018, 2020) and the same set of OpSim conditions Lochner et al. (2021) used for DESC’s assessment of the impact of OS on multi-probe cosmological constraints. As an overview, we use CMNN to generate mock photometry for a given OpSim simulation, then use the traditional photo- z metrics evaluated on CMNN’s photo- z estimates to identify exemplary OSs to which we then apply TLM.

For each OpSim OS simulation, we first determine the 5σ limiting magnitude of the 10-year coadded images from the wide-fast-deep program in sky regions (HEALpix ~ 220 arcmin wide). We identify regions as extragalactic fields (i.e., appropriate for cosmological studies) if their Galactic dust extinction was $E(B-V) < 0.2$ mag and if they received at least 5 visits per year in all six *ugrizy* filters, and

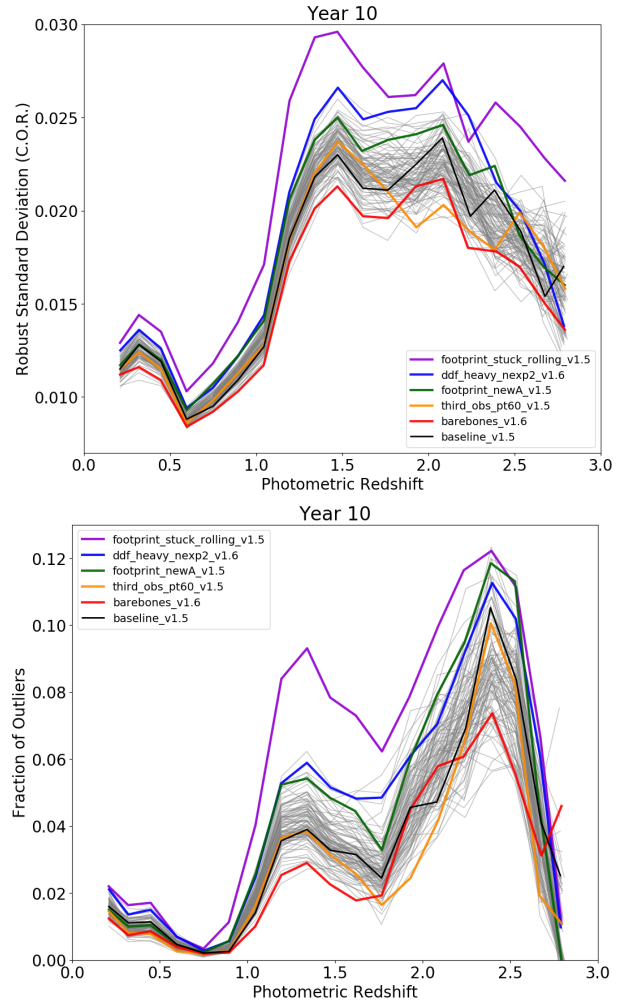


Figure 1. CMNN-estimated photo- z statistics for a wide variety of OpSim conditions (grey), the baseline OpSim (black), and the exemplary OpSim OS simulations used in this pilot study (colors as in legend). The *baseline_v1.5* OS has mid-quality results, and the simulations used in this analysis were chosen because they represent a range of photo- z qualities that stand out as better and worse than *baseline_v1.5*. These results should not be taken as representative of the future *absolute* quality of LSST photo- z , but the differences in the results are representative of the impact of different OpSim strategies on the photo- z results.

then calculate the median 10-year depths over all extragalactic fields, which are reported in Table 1. For every OpSim OS simulation, these 5σ depths in each filter, m_5 , are passed to the CMNN Estimator, which uses them to calculate magnitude errors for a catalog of mock galaxies: $\sigma_{\text{rand}}^2 = (0.04 - \gamma)x + \gamma x^2$, where $x = 0.4(m_{\text{true}} - m_5)$, m_{true} is the true catalog apparent magnitude, and γ is a filter-dependent factor which account for the effect of, e.g., sky brightness (see Section 3.2 of Ivezić et al. 2019). The CMNN Estimator then simulates observed apparent magnitudes by drawing a random value from a normal distribution with a standard deviation equal to σ_{rand} and adding it to the true catalog magnitude. Test- and training-sets are drawn randomly (without replacement) from the mock galaxy catalog, and photo- z estimates for the test set are generated by identifying training-set galaxies with similar colors, i.e. a subset of color-matched nearest-neighbors in 5-dimensional color space, and adopting as the true redshift one test-set galaxy’s photo- z chosen at random. In order to standardize the mock catalogs used for all simulations, we applied

⁵ A demonstration of the CMNN photo- z estimator is available on GitHub at https://github.com/dirac-institute/CMNN_Photoz_Estimator.

OpSim OS Simulation	m5_u	m5_g	m5_r	m5_i	m5_z	m5_y
baseline_v1.5	25.86	27.02	26.99	26.42	25.70	24.94
footprint_stuck_rolling_v1.5	25.56	26.68	26.62	26.06	25.33	24.61
ddf_heavy_nexp2_v1.6	25.57	26.82	26.84	26.26	25.57	24.82
footprint_newA_v1.5	25.75	26.87	26.85	26.29	25.55	24.78
third_obs_pt60_v1.5	25.87	27.03	26.99	26.43	25.70	24.93
barebones_v1.6	26.00	27.13	27.07	26.57	25.78	25.05

Table 1. Simulated median 5σ limiting magnitudes in extragalactic regions for coadded images from the wide-fast-deep survey, from the *baseline_v1.5* OpSim OS simulation and the five exemplary OpSim OS simulations used in this work.

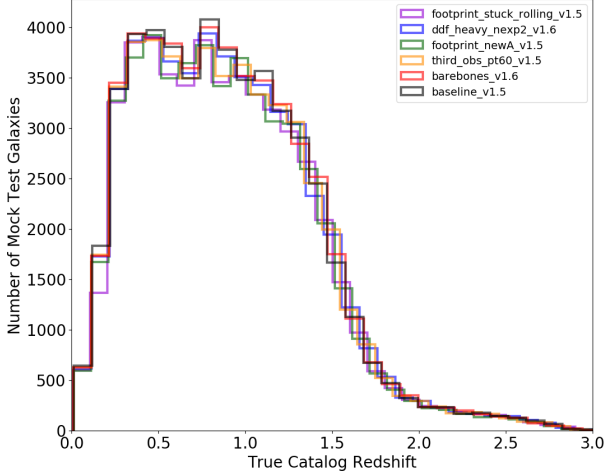


Figure 2. The true catalog redshift distribution for the mock test galaxy sets used to simulate photo- z results for each OpSim OS simulation. Differences between the redshift distributions across OpSim OS simulations are due to statistical fluctuations and correspond to a 0.5% difference in entropy $H(Z)$, meaning they are statistically indistinguishable.

the same cuts on the observed apparent magnitudes of 25.0, 26.0, 26.0, 25.0, 24.8, and 24.0 mag in filters *ugrizy* to both the test and training sets, about half a magnitude brighter than the brightest 5σ limiting depth of any given OpSim OS simulation, as in [Lochner et al. \(2021\)](#).

It is important to note that for all of our simulations, the test- and training-sets were drawn from the same intrinsic mock catalog, which means they are perfectly matched in terms of their redshift and apparent magnitude distributions. While this would be concerning if we aimed to evaluate the realistic performance of the CMNN estimator, its role in this study is not to produce LSST’s “official” or even “best” photo- z s; rather, we use it as a forward model of the relationship between the relative quality of photo- z estimates given the quality of input photometry, which provides us with mock photometry under a given OS upon which we demonstrate TLM.

Several statistical measures are commonly used to evaluate the quality of test-set photo- z estimates based on the photo- z error, $\Delta z \equiv (z_{\text{true}} - z_{\text{phot}})/(1 + z_{\text{phot}})$. While the bias $\langle \Delta z \rangle$, representing systematic over- or under-estimates of point estimates, was calculated, the values under these idealized conditions of a perfectly representative and complete training-set were too small and similar for bias to discriminate between OSs. However, our experimental design does produce simulated photo- z results for which the standard deviation and fraction of outliers are relatively improved or degraded in a way that correlates with the 5σ depths in the six LSST filters. For a robust standard deviation in Δz we use the interquartile range (IQR) divided by 1.349, making the fraction of outliers the fraction

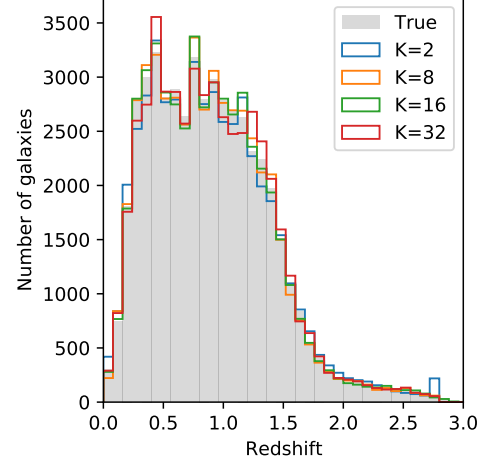


Figure 3. Histogram of the redshift distributions for *baseline_v1.5* under normalizing flows with different values of the tuning parameter K . The true distribution is in gray, while the distribution learned by normalizing flows with various values of K are displayed in color. Aside from a high-redshift artifact for the extreme $K = 2$ flow, the choice of K appears to have little effect.

of test-set galaxies with $|\Delta z| > 3 \times$ the robust standard deviation or $> 3 \times 0.06$, whichever is larger (matching the definition of the LSST Science Requirements Document, [Ivezić & the LSST Science Collaboration 2013](#)).

In Figure 1, we show the robust standard deviation and fraction of outliers⁶ in bins of photo- z for a wide variety of OpSim OS simulations, highlighting the baseline OpSim OS simulation and a selection of five additional OpSim OS simulations which produced notably better or worse results than the baseline that we use in this work, whose median 10-year depths are provided in Table 1.

In Figure 2, we show the distribution of true catalog redshift for the test-set galaxies used for each simulation. Because the same magnitude cuts were applied to the test and training sets for all simulations, the training sets have similar redshift distributions. The differences between the lines are just the statistical random fluctuations caused by drawing a new test subset (of 50000) from the greater mock galaxy catalog (of millions of galaxies) for each simulation. The drop in the number of galaxies in high redshift bins is realistic for the applied cuts on apparent magnitude, and is the cause for some of the observed scatter in the photo- z statistical results seen in Figure 1.

⁶ See [Graham et al. \(2020\)](#) for a full description of the standard deviation and fraction of outliers statistics.

3.2 Implementation: density estimation with pzflow

We build the NF lower bound discussed in Section 2.3 using pzflow (Crenshaw 2021), a GPU-enabled python package for normalizing flows built on Jax (Bradbury et al. 2018). We refer to our public implementation as TheLastMetric⁷.

For the latent distribution $p(z)$, we use the uniform distribution $\mathcal{U}(0, 3.2)$, as sampling and density estimation are trivial, and the domain matches the compact support of the redshifts in our data set. Matching the features of the latent space to the data eases training and prevents any potential unphysical outliers.

For the bijection f_φ , we use a rational-quadratic neural spline coupling (RQ-NSC; Durkan et al. 2019), which is a state-of-the-art bijection both capable of modeling high-dimensional distributions with hundreds of modes and efficient at both sampling and density estimation. The RQ-NSC transforms galaxy redshifts with monotonically-increasing piecewise combinations of K segments, each of which is a rational-quadratic function. The bijection parameters φ are the values and derivatives of these rational-quadratic functions at $K + 1$ spline knots. The value of K impacts the resolution of the distribution learned by the NF, with large K corresponding to high resolution. After fixing K , a neural network calculates the values and derivatives of the $K + 1$ knots from the conditional variables: the five LSST colors ($u - g, g - r, r - i, i - z, z - y$) and the r band magnitude (which serves as a proxy for overall luminosity). After assessing several configurations for the neural architecture of our NFs, we adopted a single RQ-NSC coupling layer, parameterized by a dense neural network with 2 layers of size 128 and ReLU non-linearities.

To confirm robustness to the choice of tuning parameter K , we train flows with $K = 2, 8, 16$, and 32 for each of the six OSs under consideration. Each flow is trained by minimizing the loss of Equation 12 with respect to the parameters φ using the Adam optimizer (Kingma & Ba 2014). We train with a learning rate (lr) of 10^{-3} for 100 epochs, followed by $\text{lr} = 2 \times 10^{-4}$ for 100 epochs, followed by $\text{lr} = 10^{-4}$ for 50 epochs. For each flow, this takes about 1 minute on a Tesla P100 12GB GPU (or about twice that on a CPU). Figure 3 shows the redshift distributions learned by the four flows trained on the *baseline_v1.5* OS. Aside from a high-redshift artifact for $K = 2$, the choice of K has little effect on the redshift distribution learned by the flow. Similar behavior is observed for the redshift distributions of the other OSs, as well as the cross-correlations with galaxy colors. Thus, for the remainder of this work, we will just use $K = 16$.

Now that we have set the value of K , for each OS we train nine additional flows with $K = 16$ and the same training schedule. The 10 flows per OS will be used as a deep ensemble (Lakshminarayanan et al. 2016) to account for the *epistemic uncertainty* of the model. Deep ensembles perform approximate Bayesian marginalization (Wilson & Izmailov 2020) over network parameters by independently initializing and training neural network parameters a number of different times. In the case of a non-convex loss function, this procedure often results in solutions that live in distinct basins of attraction in parameter space (Fort et al. 2020) and is therefore preferable to methods that approximately marginalize over single basins of attraction, such as the Laplace (MacKay 1992) and SWAG (Maddox et al. 2019) approximations. We calculate a distribution and report a mean of \mathfrak{n} for each OS based on the ten trained NFs.

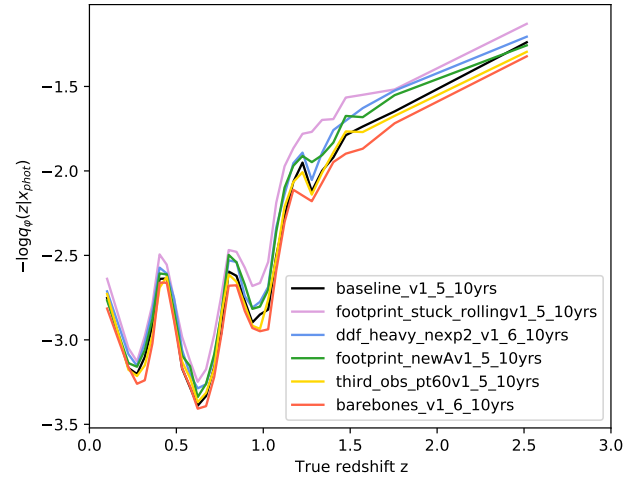


Figure 4. Redshift-binned average of negative log-posterior $-\log q_\varphi(z|x_{\text{phot}})$ under each OpSim OS simulation, analogous to Figure 1 (i.e. lower is better). This component of TLM indicates the uncertainty on redshifts given observed photometry, for instance, the reduction in redshift uncertainty as the Balmer break passes between the LSST photometric filters, and otherwise follows the dominant trend of the traditional photo- z metrics by worsening at high redshift. Though the general ranking of OSs matches that of the traditional metrics, the reorderings between redshift bins is not as severe, an indication of robustness of TLM.

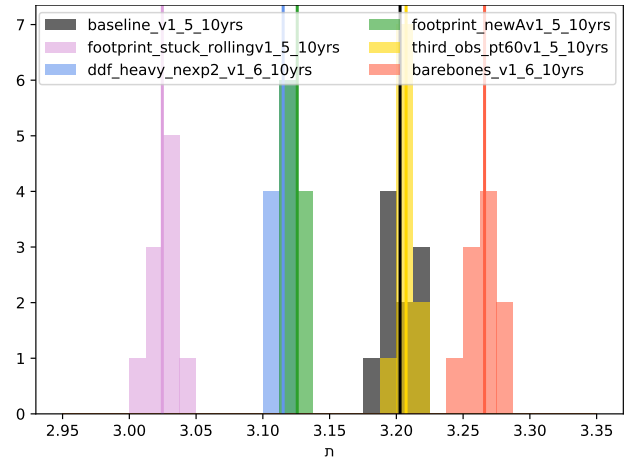


Figure 5. The distribution of \mathfrak{n} estimates for each OS. The shaded distributions represent an estimate of the epistemic errors in the evaluation of the metric, obtained using a deep ensemble approach. Mean \mathfrak{n} estimates indicated by vertical lines are obtained by averaging of the deep ensemble values. The stochasticity exceeds the difference between metric values for two pairs of OSs, but stratification by TLM is otherwise robust.

3.3 Results

As a hypothesis, we expect that TLM will confirm the hierarchy of OSs corresponding to the traditional photo- z statistics; as will be discussed in Section 4, the advantages of TLM are its potential extensions, but we first establish its consistency with our intuition based on the established photo- z metrics.

Before considering TLM's value for each OS, we aim to build some intuition of how it behaves in practice. We therefore begin by considering the behavior of a key component of \mathfrak{n} : the per-galaxy log-posterior $\log q_\varphi(z|x_{\text{phot}})$, which quantifies how probable the true redshift of a galaxy with photometry x_{phot} is under the ap-

⁷ <https://github.com/aimalz/TheLastMetric>

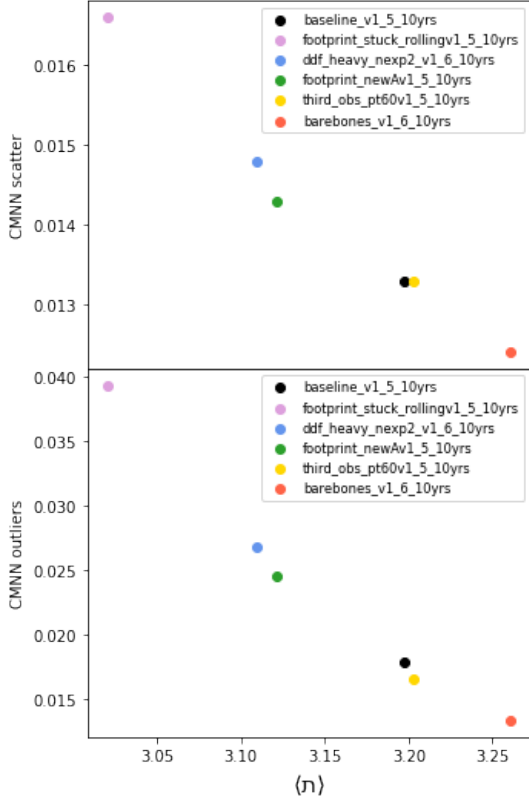


Figure 6. A comparison between the mean \mathfrak{I} and the traditional photo- z metrics of intrinsic scatter (top panel) and outlier rate (bottom panel) from the CMNN estimator, calculated for the redshift range $0.3 < z_{\text{phot}} < 3.0$ for each OS (colors). Both TLM and traditional photo- z metrics penalize the *footprint_stuck_rolling_v1.5* and *ddf_heavy_nexp2_v1.6* OSs and favor *barebones_v1.6* and generally agree on the ranking of OSs.

proximated posterior redshift distribution. This value would be high for narrow posteriors centered on the true redshifts, indicating that the photometry is very constraining of redshift. Alternatively, a low value indicates that the posterior is not very concentrated and/or offset from the true redshift, meaning that the photometry is not very constraining.

Figure 4 shows the redshift-binned negative expected value $\langle -\log q_{\varphi}(z|x_{\text{phot}}) \rangle$ for different OSs; the minus sign is included for easier comparison with Figure 1, i.e. lower is better. We confirm the conclusions of the CMNN statistics of Figure 1: towards higher redshifts, photometry becomes less constraining, in the same way that the scatter and outlier rate increases for CMNN, and the *barebones_v1.6* OS consistently outperforms the *footprint_stuck_rolling_v1.5* OS at all redshifts. We also observe from Figure 4 that the ordering of OSs by these curves does not significantly depend on redshift, which is largely consistent with the findings of the traditional metrics of Figure 1. This indicates that there is not a sub-range of redshifts for which a given strategy would outperform the others, which implies that a single OS could be optimal for both low-redshift and high-redshift science use cases.

In addition, $\langle -\log q_{\varphi}(z|x_{\text{phot}}) \rangle$ achieves a series of local minima, corresponding to increased information content, around the redshifts where the 4000 Å Balmer break, a broad feature of galaxy spectra important for photo- z estimation, crosses between the LSST photometric filters. This provides a strong consistency check that our implementation of the metric is capturing the real, physical mutual

information between photometry and redshift. It also demonstrates consistency with the results of Kalmbach et al. (2020), who found that using information theory to optimize filters for photo- z s corresponds to designing filters that can optimally constrain the location of the Balmer break as it moves across the optical wavelength range.

As described in Section 2.2, \mathfrak{I} itself is obtained by taking the expectation of the log-posterior $\log q_{\varphi}(z|x_{\text{phot}})$ over the entire sample, thus capturing how informative the observed photometry is about the redshifts across the whole population, and adding an entropy term $H(Z)$ which only depends on the redshift distribution.

The distribution of \mathfrak{I} from the deep ensembles for each OS are shown in Figure 5, recalling that higher \mathfrak{I} is better. The epistemic uncertainty in TheLastMetric dominates \mathfrak{I} 's discriminatory power for two pairs of OSs, but there is a clear four-tiered hierarchy of the redshift information each OS's photometry preserves.

Figure 6 shows the mean values $\langle \mathfrak{I} \rangle$ of these distributions, plotted against the two relevant canonical photo- z metrics of Figure 1 for each OS, confirming that the behavior of \mathfrak{I} is qualitatively similar to that of the traditional photo- z metrics⁸, favoring *barebones_v1.6* and disfavoring *footprint_stuck_rolling_v1.5*.

4 DISCUSSION & CONCLUSIONS

In this paper, we introduce *TheLastMetric*, \mathfrak{I} , a metric of mutual information, and apply it in the context of observing strategy optimization for an astronomical survey with diverse scientific goals. We also present TheLastMetric to the community, an implementation of a variational lower bound on the mutual information of photometry with respect to redshift. We demonstrate the calculation of *TheLastMetric* on mock photometric galaxy catalogs corresponding to exemplary observing strategies for LSST, confirming that it is qualitatively similar to conventional photo- z metrics.

TheLastMetric offers distinct advantages addressing key needs for observing strategy metrics for LSST's diverse extragalactic goals:

- *TheLastMetric* is a measure of information in units of nats, meaning it and any science-case specific extensions thereof are directly comparable, enabling the isolation of the relative importance of science goals from the raw values of their observing strategy metrics.
- TheLastMetric does not assume any photo- z estimator, freeing it from assumptions of photo- z template libraries, training sets, and other priors, as well as from the computational overhead associated with many popular photo- z estimators.
- *TheLastMetric* is applicable across redshift-dependent science cases as well as to other quantities informed by photometry that is influenced by observing strategy.

TheLastMetric is not without its own assumptions of course. We show that it is robust to the tuning parameters of the TheLastMetric back-end, but evaluation on draws from the conditional normalizing flow model rather than the same data upon which it was trained would, strictly speaking, be more self-consistent. Furthermore, though TheLastMetric eliminates the computational expense of estimating photo- z s, it retains the traditional metrics' computational overhead of simulating a mock galaxy catalog from OpSim parameters.

We note that the entropy $H(Z)$ of the redshift distribution of the

⁸ It also confirms the close correlation between the traditional intrinsic scatter and outlier rate, as the latter is defined in terms of the former.

mock galaxy catalog, which factors into \mathfrak{N} in Equation 9 and thus influences Figures 5 and 6, may differ between cosmological probes or other science cases that use subsamples of galaxies under different selection functions. Though the entropy term $H(Z)$ would need to be recomputed for the anticipated redshift distribution of the science-motivated subsample, that term is subdominant in magnitude as well as trivial to calculate. Since the expected value of Equation 9 is defined in terms of $p(z, x_{phot})$, \mathfrak{N} could be recalculated under a different redshift distribution without requiring retraining of *TheLastMetric* to obtain the $\log q_{\phi}(z|x_{phot})$ for each mock galaxy. Thus *TheLastMetric* is extensible to redshift-dependent science cases without increasing computational expense beyond what is required of the current photo- z metrics.

Mathematically, *TheLastMetric* is not inherently exclusive to redshift and may be extended to any parameter of interest available in the truth catalog of a mock galaxy sample to yield an interpretable metric of how informative the photometry is about that parameter. Use of *TheLastMetric* and potential extensions thereof, within and beyond cosmological applications, will enable the identification of an appropriate observing strategy for LSST. We thus recommend *TheLastMetric*'s inclusion in the MAF and motivate future development into further mutual information metrics specific to individual science cases or probes of a single science application.

ACKNOWLEDGEMENTS

This work was incubated at the August 2020 TVS SC MAF Hackathon⁹, which was supported by an LSSTC Enabling Science small programs grant.

AIM acknowledges support from the Max Planck Society and the Alexander von Humboldt Foundation in the framework of the Max Planck-Humboldt Research Award endowed by the Federal Ministry of Education and Research. JFC is supported by the U.S. Department of Energy, Office of Science, under Award DE-SC-0011635, as well as the National Science Foundation, Division Of Astronomical Sciences, under Award AST-1715122, and the Office of Advanced Cyberinfrastructure, under Award OAC-1739419. MLG acknowledges support from the DIRAC Institute in the Department of Astronomy at the University of Washington. The DIRAC Institute is supported through generous gifts from the Charles and Lisa Simonyi Fund for Arts and Sciences, and the Washington Research Foundation.

REFERENCES

- Alemi A., Fischer I., Dillon J., Murphy K., 2017, in ICLR. <https://arxiv.org/abs/1612.00410>
- Almoubayyed H., et al., 2020, Monthly Notices of the Royal Astronomical Society, 499, 1140
- Awan H., et al., 2016, ApJ, 829, 50
- Bachman P., Devon Hjelm R., Buchwalter W., 2019, arXiv e-prints, [p. arXiv:1906.00910](https://arxiv.org/abs/1906.00910)
- Barber D., Agakov F., 2003, in Proceedings of the 16th International Conference on Neural Information Processing Systems. NIPS'03. MIT Press, Cambridge, MA, USA, p. 201–208
- Bradbury J., et al., 2018, JAX: composable transformations of Python+NumPy programs, [http://github.com/google/jax](https://github.com/google/jax)
- Chang C., et al., 2018, Mon Not R Astron Soc, 482, 3696
- Cover T. M., Thomas J. A., 2006, ELEMENTS OF INFORMATION THEORY. Telecommunication, Wiley

- Crenshaw J. F., 2021, [jfcrenshaw/pzflow: v1.6.0, doi:10.5281/zenodo.4679913, https://doi.org/10.5281/zenodo.4679913](https://doi.org/10.5281/zenodo.4679913)
- Delgado F., Saha A., Chandrasekharan S., Cook K., Petry C., Ridgway S., 2014, in Modeling, Systems Engineering, and Project Management for Astronomy VI. International Society for Optics and Photonics, p. 915015
- Dinh L., Krueger D., Bengio Y., 2015, in Bengio Y., LeCun Y., eds, Proceedings of the 3rd International Conference on Learning Representations. San Diego, CA ([arXiv:1410.8516](https://arxiv.org/abs/1410.8516))
- Durkan C., Bekasov A., Murray I., Papamakarios G., 2019, in Wallach H. M., Larochelle H., Beygelzimer A., d'Alché-Buc F., Fox E. B., Garnett R., eds, Advances in Neural Information Processing Systems 32. Curran Associates, Inc., Vancouver, Canada, pp 7511–7522 ([arXiv:1906.04032](https://arxiv.org/abs/1906.04032))
- Fort S., Hu H., Lakshminarayanan B., 2020, arXiv:1912.02757 [cs, stat]
- Goodfellow I. J., Pouget-Abadie J., Mirza M., Xu B., Warde-Farley D., Ozair S., Courville A., Bengio Y., 2014, arXiv e-prints, [p. arXiv:1406.2661](https://arxiv.org/abs/1406.2661)
- Górski K. M., Hivon E., Banday A. J., Wandelt B. D., Hansen F. K., Reinecke M., Bartelmann M., 2005, ApJ, 622, 759
- Graham M. L., Connolly A. J., Ivezić Ž., Schmidt S. J., Jones R. L., Mario Jurić Daniel S. F., Yoachim P., 2018, AJ, 155, 1
- Graham M. L., et al., 2020, AJ, 159, 258
- Ivezić Ž., the LSST Science Collaboration 2013, <http://ls.st/LPM-17>
- Ivezić Ž., et al., 2019, ApJ, 873, 111
- Jimenez Rezende D., Mohamed S., 2015, arXiv e-prints, [p. arXiv:1505.05770](https://arxiv.org/abs/1505.05770)
- Jones R. L., Yoachim P., Ivezić Z., Neilsen E. H., Ribeiro T., 2020, Technical Report 051, Survey Strategy and Cadence Choices for the Vera C. Rubin Observatory Legacy Survey of Space and Time (LSST). LSST
- Kalmbach J. B., VanderPlas J. T., Connolly A. J., 2020, The Astrophysical Journal, 890, 74
- Kingma D. P., Ba J., 2014, arXiv e-prints, [p. arXiv:1412.6980](https://arxiv.org/abs/1412.6980)
- Kingma D. P., Welling M., 2013, arXiv e-prints, [p. arXiv:1312.6114](https://arxiv.org/abs/1312.6114)
- Kobyzev I., Prince S. J. D., Brubaker M. A., 2020, IEEE Transactions on Pattern Analysis and Machine Intelligence, pp 1–1
- LSST 2016, OpSim 3.3.8
- LSST 2017, MAF 2.4.0
- LSST Science Collaboration et al., 2017, arXiv e-prints, [p. arXiv:1708.04058](https://arxiv.org/abs/1708.04058)
- Lakshminarayanan B., Pritzel A., Blundell C., 2016, arXiv e-prints, [p. arXiv:1612.01474](https://arxiv.org/abs/1612.01474)
- Lochner M., et al., 2018, arXiv:1812.00515 [astro-ph]
- Lochner M., et al., 2021, arXiv:2104.05676 [astro-ph]
- MacKay D. J., 1992, PhD thesis, California Institute of Technology
- Maddox W., Garipov T., Izmailov P., Vetrov D., Wilson A. G., 2019, arXiv:1902.02476 [cs, stat]
- Malz A. I., Marshall P. J., DeRose J., Graham M. L., Schmidt S. J., Wechsler R., Collaboration) L. D. E. S., 2018, AJ, 156, 35
- Poole B., Ozair S., van den Oord A., Alemi A. A., Tucker G., 2019, CoRR, abs/1905.06922
- Schmidt S. J., et al., 2020, Mon Not R Astron Soc, 499, 1587
- Scolnic D. M., et al., 2018, arXiv:1812.00516 [astro-ph]
- Tishby N., Zaslavsky N., 2015, CoRR, abs/1503.02406
- Wilson A. G., Izmailov P., 2020, arXiv:2002.08791 [cs, stat]
- Winkler C., Worrall D., Hoozeboom E., Welling M., 2019, arXiv:1912.00042 [cs, stat]

This paper has been typeset from a \LaTeX file prepared by the author.

⁹ <https://lsst-tvssc.github.io/metricshackathon2020>